J|A|C|S
ARTICLES
Published on Web 08/23/2002

Hybrid Density Functional Theory Studies on the Magnetic Interactions and the Weak Covalent Bonding for the Phenalenyl Radical Dimeric Pair

Yu Takano,*,† Takeshi Taniguchi,† Hiroshi Isobe,† Takashi Kubo,† Yasushi Morita,† Kagetoshi Yamamoto,† Kazuhiro Nakasuji,† Takeji Takui,‡ and Kizashi Yamaguchi*,†

Contribution from the Department of Chemistry, Graduate School of Science, Osaka University, Toyonaka, Osaka 560-0043, Japan, and Department of Chemistry, Graduate School of Science, Osaka City University, Sumiyoshi-ku, Osaka 558-8585, Japan

Received December 10, 2001

Abstract: The phenalenyl radical (**1**) is a prototype of the hydrocarbon radical. Recently, the single crystal of 2,5,8-tri-*tert*-butylphenalenyl (**2**) was isolated and showed that the two phenalenyl radicals form a staggered dimeric pair, giving rise to strong antiferromagnetic interactions. The origin of the antiferromagnetic interactions and the nature of the chemical bond for the dimeric pair are challenging issues for chemists. First, spin-polarized hybrid DFT (Becke's half and half LYP (UB2LYP)) and CASSCF calculations were performed for **2** and its simplified model, the staggered-stacking phenalenyl radical dimeric pair (**3a**), to elucidate the origin of the strong antiferromagnetic coupling and the characteristics of the chemical bond. The calculated results showed that a SOMO−SOMO overlap effect was responsible for the strong antiferromagnetic interactions and weak or intermediate covalent bonding between phenalenyl radicals. The *tert*-butyl groups introduced at three β-positions hardly affected the magnetic coupling, mainly causing steric hindrances in the crystalline state. Next, to obtain insight into ferromagnetic stacking, we investigated the stacking effect of staggered (**3a**)- and eclipsed (**3b**)-stacking phenalenyl radical dimeric pairs with a change of the SOMO−SOMO overlap on the basis of the extended McConnell model. We found that the stacking mode of the dimeric pair with both a small SOMO−SOMO overlap and a ferromagnetic spin polarization effect provided a ferromagnetic coupling.

Introduction

Phenalenyl is an odd-alternant hydrocarbon with high symmetry, D_{3h}, and is stable in solution under an inert gas atmosphere.[1] The molecule has the ability to form three redox species: cation, radical **1**, and anion as shown in Figure 1. Such characteristic features have been utilized for exploring new conjugated electronic systems such as electronically and magnetically intriguing materials.[2] Especially, phenalenyl radicals are expected to be the building blocks of molecule-based magnets.[2] Although the hydrocarbon radicals are prototypes of radicals, no phenalenyl radicals in the solid state were characterized in detail because of their ease in dimerization and/or oxidation by air. Stable phenalenyl π radicals have recently been isolated by introduction of *tert*-butyl groups at three β positions because the highly reactive phenalenyl radical requires substituents for kinetic stabilization.[3] X-ray crystallographic analysis[3] showed that the molecules formed a dimeric pair **2** in the monoclinic crystal ($P2_1/n$, $Z = 4$), as illustrated in Figure 1. In the dimeric pair, the two radicals face each other with an interplane distance of about 3.3 Å, where one is related to the other by an inversion symmetry. A superconducting quantum interface devices (SQUID) study[4,5] suggested that the dimeric pair showed the strong antiferromagnetic interactions ($2J_{ab} = -1318$ cm^{-1}). Judging from the C−C distance ($R = 3.3$ Å), we found that **2** should show a singlet diradical character, that is, an intermediate bond character between covalent bonding and dissociation.

The aims of our study are (1) to elucidate the origin of the effective exchange interaction (J_{ab}) and the nature of the chemical bond and (2) to find the ferromagnetic stacking for the phenalenyl radical dimeric pair. First, we carried out spin-polarized Becke's half and half LYP (UB2LYP) calculations[6,7] for the 2,5,8-tri-*tert*-butylphenalenyl radical dimeric pair **2** and

* To whom correspondence should be addressed. (Y.T.) Phone: +81-6-6850-5405. Fax: +81-6-6850-5550. E-mail: ytakano@chem.sci.osaka-u.ac.jp. (K.Y.) Phone: +81-6-6850-5405. Fax: +81-6-6850-5550. E-mail: yama@chem.sci.osaka-u.ac.jp.

† Osaka University.

‡ Osaka City University.

(1) Reid, D. H. *Q. Rev.* **1965**, *19*, 274.

(2) (a) Koutentis, P. A.; Chen, Y.; Cao, Y.; Best, T. P.; Itkis, M. E.; Beer, L.; Oakley, R. T.; Cordes, A. W.; Brock, C. P.; Haddon, R. C. *J. Am. Chem. Soc.* **2001**, *123*, 3864. (b) Itkis, M. E.; Chi, X.; Cordes, A. W.; Haddon, R. C. *Science* **2002**, *296*, 1443.

(3) Goto, K.; Kubo, T.; Yamamoto, K.; Nakasuji, K.; Sato, K.; Shiomi, D.; Takui, T.; Kubota, M.; Kobayashi, T.; Yakushi, K.; Ouyang, J. *J. Am. Chem. Soc.* **1999**, *121*, 1619.

(4) Fukui, K.; Sato, K.; Shiomi, D.; Takui, T.; Itoh, K.; Gotoh, K.; Kubo, T.; Yamamoto, K.; Nakasuji, K.; Naito, A. *Synth. Met.* **1999**, *103*, 2257.

(5) Fukui, K.; Sato, K.; Shiomi, D.; Takui, T.; Itoh, K.; Kubo, T.; Gotoh, K.; Yamamoto, K.; Nakasuji, K.; Naito, A. *Mol. Cryst. Liq. Cryst.* **1999**, *334*, 49.

(6) (a) Hohenberg, P.; Kohn, W. *Phys. Rev. B* **1964**, *136*, 864. (b) Kohn, W.; Sham, L. *Phys. Rev. A* **1965**, *140*, 1133. (c) Parr, R. G.; Young, W. *Density Functional Theory of Atoms and Molecules*; Oxford University Press: Oxford, 1989.

(7) Becke, A. D. *J. Chem. Phys.* **1993**, *98*, 1372.

10.1021/ja0177197 CCC: $22.00

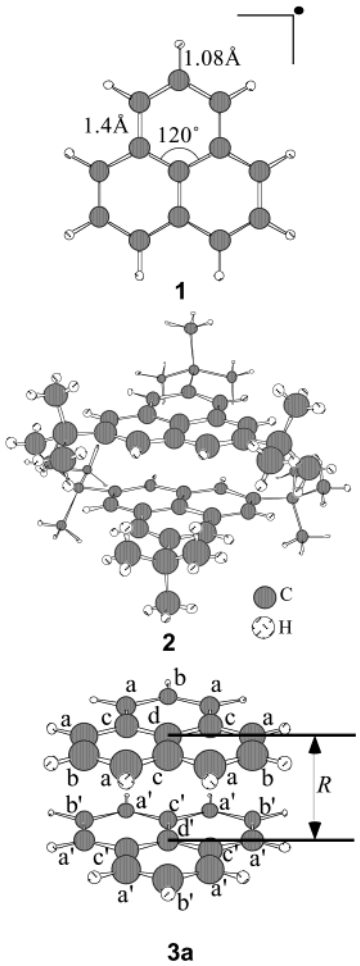

Figure 1. Geometries of phenalenyl radical monomer (**1**), 2,5,8-tri-*tert*-butylphenalenyl radical dimeric pair (**2**), and staggered-stacking phenalenyl radical dimeric pair (**3a**). Site indices a (a′)−d (d′) are shown in **3a**.

a simplified model **3a** as shown in Figure 1. Complete active space self-consistent field (CASSCF) calculations[8] for **3a** were also performed to elucidate a contribution of the singly occupied MO (SOMO)−SOMO overlap effect. The J_{ab} values, the spin density distributions, and the shape and symmetry of the molecular orbitals (MOs) for **2** and **3a** indicated that SOMO−SOMO overlap effects caused the strong antiferromagnetic couplings and that the diradical characters were recognized as the intermediate character between bond dissociation and covalent bonding. Next, to obtain organic molecule-based ferromagnets, the stacking effects on the magnetic interactions for the phenalenyl radical dimeric pair were examined. UB2LYP and CASSCF calculations were performed for the staggered (**3a**)- and eclipsed (**3b**)-stacking phenalenyl radical dimeric pairs with a change of the SOMO−SOMO overlap on the basis of the extended McConnell model.[9] We found that the stacking modes with the small SOMO−SOMO overlap and the ferromagnetic intermolecular spin alignment provided organic ferromagnetic crystals.

Theoretical Background

Effective Exchange Interactions (J_{ab}). Magnetism is one of the characteristic properties in strong electron correlated systems. Dimeric pairs **2** and **3** are regarded as such systems. It is necessary to perform post Hartree−Fock (HF) calculations including dynamical correlation corrections to investigate the magnetic interaction for the dimeric pair; however, it is difficult to do these calculations for large systems. In recent years, density functional (DFT) calculations[6] have been performed for large and strong correlated systems to understand diradical characters. DFT has been accepted as an alternative approach for the post HF methods to overcome the electron correlation problem for large systems.

We previously[10] performed unrestricted HF (UHF),[11] pure DFT (UBLYP),[12] hybrid DFT (UB2LYP[7] and UB3LYP[13]), and post HF calculations for the organic polyradicals and magnetic polymers cross-linked by *m*-phenylene groups to investigate the nature of the effective exchange interactions. We concluded that the spin polarization effects via chemical bonds, through-bond, were responsible for the magnetic interactions and that DFT employing appropriate exchange-correlation functionals was practically useful for the estimate of the electronic and magnetic properties of these species. On the other hand, **2** shows an intermolecular (through-space) antiferromagnetic interaction. We need to investigate the intermolecular magnetic couplings for **2**.

The effective exchange interactions between the phenalenyl radicals can be described with the Heisenberg model:

$$H = -2\sum J_{ab}\mathbf{S_a}\cdot\mathbf{S_b} \qquad (1)$$

where $\mathbf{S_a}$ and $\mathbf{S_b}$ represent the spins at sites a and b, respectively. J_{ab} is an effective exchange integral. We considered each radical as a spin site to estimate J_{ab} values for the molecule-based magnet. In this study, we estimated the J_{ab} values with UB2LYP calculations. It is known that UB2LYP solutions for the lowest spin (LS) state usually exhibit broken symmetry problems.[14] Therefore, an approximate spin projection (AP) procedure for the broken symmetry solutions should be carried out to eliminate spin contaminations in UB2LYP. The J_{ab} values can be calculated using a combination of the total energies in the highest spin (HS) and LS states by UB2LYP with the Heisenberg model[15] as

$$J_{ab} = \frac{{}^{LS}E_X - {}^{HS}E_X}{{}^{HS}\langle S^2\rangle_X - {}^{LS}\langle S^2\rangle_X} \qquad (2)$$

(8) (a) Roos, B. O. Methods in Computational Molecular Physics. In *The Multiconfiguration SCF Method*; Diercksen, G. H. F., Wilson, S., Eds.; D. Reidel Publishing: Dordrecht, Netherlands, 1983; p 161. (b) Yamaguchi, K. *Int. J. Quantum Chem. Symp.* **1980**, *14*, 269. (c) Yamanaka, S.; Okumura, M.; Yamaguchi, K.; Hirao, K. *Chem. Phys. Lett.* **1994**, *225*, 213.
(9) (a) McConnell, H. M. *J. Chem. Phys.* **1963**, *39*, 1910. (b) Yamaguchi, K.; Fueno, T.; Nakasuji, K.; Murata, I. *Chem. Lett.* **1986**, 629. (c) Yamaguchi, K.; Fueno, T. *Chem. Phys. Lett.* **1989**, *159*, 465. (d) Kawakami, T.; Yamanaka, S.; Yamada, S.; Mori, W.; Yamaguchi, K. *Molecule-Based Magnetic Materials, Theory, Technique, and Applications*; ACS Symposium Series 644, 1996; p 30.
(10) (a) Mitani, M.; Mori, H.; Takano, Y.; Yamaki, D.; Yoshioka, Y.; Yamaguchi, K. *J. Chem. Phys.* **2000**, *113*, 4035. (b) Mitani, M.; Yamaki, D.; Takano, Y.; Kitagawa, Y.; Yoshioka, Y.; Yamaguchi, K. *J. Chem. Phys.* **2000**, *113*, 10486. (c) Mitani, M.; Takano, Y.; Yoshioka, Y.; Yamaguchi, K. *J. Chem. Phys.* **1999**, *111*, 1309.
(11) Szabo, A.; Ostlund, N. S. *MODERN QUANTUM CHEMISTRY Introduction to Advanced Electronic Structure Theory*; McGraw-Hill: New York, 1989; p 205.
(12) (a) Becke, A. D. *Phys. Rev. A* **1988**, *38*, 3098−3100. (b) Lee, C.; Yang, W.; Parr, R. G. *Phys. Rev. B* **1988**, *37*, 785.
(13) Becke, A. D. *J. Chem. Phys.* **1993**, *98*, 5648.
(14) (a) Yamaguchi, K. *Chem. Phys. Lett.* **1975**, *33*, 330. (b) Yamaguchi, K. *Chem. Phys. Lett.* **1979**, *66*, 395.

where ${}^{Y}E_X$ and ${}^{Y}\langle S^2\rangle_X$ denote the total energy and total angular momentum in the spin state Y by method X, respectively.

Our AP procedure[16] can also be applied to estimate the total energy in the LS state as

$$ {}^{AP-LS}E_X = {}^{LS}E_X + J_{ab}(AP - X)[{}^{LS}\langle S^2\rangle_X - S_{min}(S_{min}+1)] \quad (3)$$

where S_{min} is the spin angular momentum in the pure LS state. This equation is derived from removal of a major part of the spin contamination errors, allowing us to depict the whole potential energy curves.[16,17]

Symmetry-adapted methods, such as CASSCF, are applicable to clarify spin alignment mechanisms. The results from CASSCF {2, 2} indicate the estimation of the contributions of the SOMO−SOMO overlap effect to J_{ab} values. CASSCF {6, 6} is performed to evaluate the indirect contribution via π-orbitals of phenalenyl radicals such as spin polarization and electron correlation effects. Inclusion of all π-orbitals of **2** and **3** is needed to estimate the spin polarization and electron correlation effects induced by π-electrons and π-orbitals of phenalenyl radicals. In other words, we should perform CASSCF {26, 26} calculations followed by the CASSCF-based second-order perturbation (CASPT2) calculations to estimate the contributions of σ-electrons; however, it is difficult in our computational systems. The J_{ab} values can be calculated using the energy gap between symmetry-adapted LS and HS states as follows:

$$ J_{ab}(CAS) = \frac{{}^{LS}E_{CAS} - {}^{HS}E_{CAS}}{S_{HS}(S_{HS}+1) - S_{LS}(S_{LS}+1)} \quad (4)$$

where ${}^{Y}E_{CAS}$ denotes the total energy by CASSCF methods in the spin state Y, and $S_{HS} = 1$ and $S_{LS} = 0$ for **3**. Equation 2 is reduced to eq 4 if the spin contamination in UB2LYP is small.

Extended McConnell Model. We proposed the extended McConnell model to show the appropriate way to build ferromagnetic organic crystals.[9] On the basis of the model, the J_{ab} values can approximately be divided into the orbital-overlap (OO), the spin density product (SDP), and higher-order terms:

$$ J_{ab} = J_{ab}(OO) + J_{ab}(SDP) + J_{ab}(higher\text{-}order) \quad (5)$$

The higher-order term can be neglected here. The OO term is governed by the sum of the orbital overlaps between the radical orbitals. For **2** and **3**, it is approximately given by the SOMO−SOMO overlaps. The SDP term is approximately provided by the spin densities on the aromatic rings, which are responsible for the intermolecular Hund's and spin polarization effects.[9c] The OO term usually contributes to the strong antiferromagnetic interactions, while the SDP term exhibits the ferro- or antiferromagnetic interactions depending on stacking modes of radicals.[10]

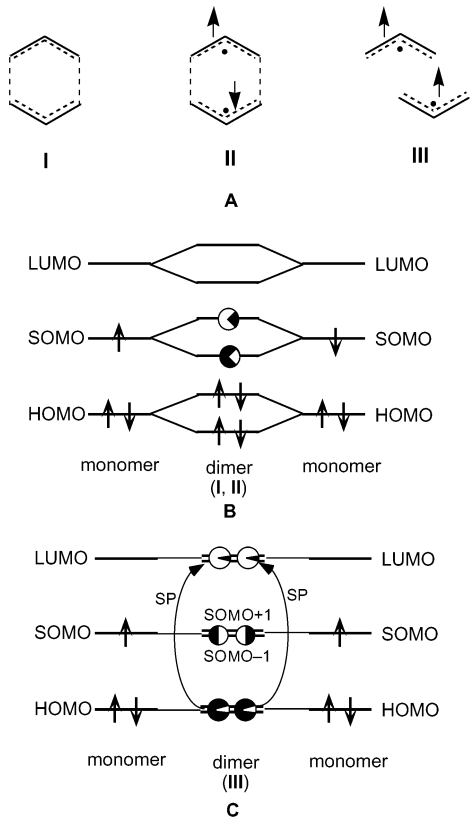

Figure 2. Diradical characters of face-to-face (**I** and **II**) and zigzag (**III**) allyl radical dimers (A), and schematic pictures of orbital interaction schemes for face-to-face (B) and zigzag allyl radical dimer (C).

Theoretical Descriptions of Diradical Species in Relation to the Magnetic Couplings. Theoretical descriptions of diradical species have attracted current interests in relation to molecular design of high-spin polyradicals and organic ferromagnets.[2,18] As an example, let us consider the face-to-face and zigzag dimers of allyl radical as illustrated in Figure 2A. The bonding and antibonding MOs of the dimer are formed from three π-molecular orbitals (MO): HOMO, SOMO, and LUMO[9c] of allyl radical as displayed in Figure 2. If the SOMO−SOMO overlap effect is strong in the dimer, the splitting in orbital energy between bonding and antibonding MOs becomes large, and both α- and β-spin electrons enter the bonding MO of the dimer (**I**) as shown in Figure 2B. If the energy gap is small, electrons partially enter the antibonding MO of the dimer, as illustrated by the shaded circle in Figure 2B, leading to the partial covalent bonding state (**II**) which still guarantees the greater stability of the singlet diradical than the triplet one. If the SOMO−SOMO overlap effect is negligible because of the orthogonality of the SOMOs, the MOs of the dimer are nearly degenerated in energy as illustrated in Figure 2C. In such a case, electrons enter the MOs in a parallel manner because of Hund's rule, affording the triplet diradical states (**III**). Moreover, when the energy gap between the singlet and triplet states (ΔE_{ST}) is relatively small, we should consider the secondary interactions, such as the spin polarization effect, as shown in Figure 2C.[9,18] The electrons in the HOMOs of the dimer are partially transferred to the LUMOs because of the polarization effect by

(15) (a) Yamaguchi, K.; Takahara, Y.; Fueno, T. In *Applied Quantum Chemistry*; Smith, V. H., Schafer, F., III, Morokuma, K., Eds.; D. Reidel: Boston, MA, 1986; p 155. (b) Yamaguchi, K.; Jensen, F.; Dorigo, A.; Houk, K. N. *Chem. Phys. Lett.* **1988**, *149*, 537. (c) Yamanaka, S.; Kawakami, T.; Nagao, H.; Yamaguchi, K. *Chem. Phys. Lett.* **1994**, *231*, 25. (d) Soda, T.; Kitagawa, Y.; Onishi, T.; Takano, Y.; Shigeta, Y.; Nagao, H.; Yoshioka, Y.; Yamaguchi, K. *Chem. Phys. Lett*. **2000**, *319*, 223.

(16) (a) Takahara, Y.; Yamaguchi, K.; Fueno, T. *Chem. Phys. Lett.* **1989**, *157*, 211. (b) Takahara, Y.; Yamaguchi, K.; Fueno, T. *Chem. Phys. Lett.* **1989**, *158*, 95.

(17) Takano, Y.; Kubo, S.; Onishi, T.; Isobe, H.; Yoshioka, Y.; Yamaguchi, K. *Chem. Phys. Lett.* **2001**, *335*, 395.

(18) (a) Yamaguchi, K.; Toyoda, Y.; Fueno, T. *Synth. Met.* **1987**, *19*, 81. (b) Yamaguchi, K.; Okumura, M.; Maki, J.; Noro, T. *Chem. Phys. Lett.* **1993**, *207*, 9.

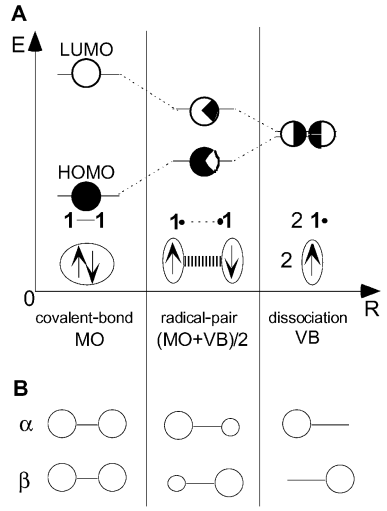

Figure 3. Schematic pictures of HOMO−LUMO gaps, bonding, orbital interactions (A), and the α and β SOMOs (B) of two H atoms in covalent-bond, radical-pair, and dissociation regions.

unpaired electrons in the SOMOs. The spin polarization effect often plays an important role in determination of the ΔE_{ST}. The ΔE_{ST}'s of diradical species are generally determined by subtle balances among the SOMO−SOMO overlap effect, Coulombic exchange (Hund's Rule), spin polarization effect, and so on.

Natural Orbital (NO) Analysis and Effective Bond Order. To develop a MO-theoretical explanation of the diradical species, the NOs of broken symmetry DFT solutions are determined by diagonalizing their first-order density matrices[19] as

$$\rho(\mathbf{r},\mathbf{r}') = \sum n_i \phi_i^*(\mathbf{r})\phi_i(\mathbf{r}') \tag{6}$$

where n_i denotes the occupation number of NO ϕ_i. The NO analysis of DFT solutions for **2** and **3** was performed to elucidate relative contributions of the spin polarization effect and the SOMO−SOMO overlap effect to J_{ab} values. The bonding magnetic orbitals $\psi_i^{\pm}$ are generally given by the linear combinations of the bonding (ϕ) and antibonding (ϕ^*) DFT NO (DNO); $\psi_i^{\pm} = \cos\theta\phi_i \pm \sin\theta\phi_i^*$, where θ is the orbital mixing coefficient.[19,20] The orbital overlap T_i between magnetic orbitals can be provided with ψ_i^+ and ψ_i^-; $T_i = \langle\psi_i^+|\psi_i^-\rangle$. The occupation numbers of the bonding and antibonding DNO are expressed with T_i:[19,20]

$$n_i = 1 + T_i, \quad n_i^* = 1 - T_i \tag{7}$$

The n_i and n_i^* values are 2.0 and 0.0 for the closed-shell pair ($T_i = 1.0$), as illustrated by black and white circles in Figures 2 and 3, while the partial covalent bond is described by partially occupied circles. The T_i values, which are estimated in terms of the n_i and n_i^* values of DNO, are equally defined by symmetry-adapted CASSCF.

The intermolecular distance R can be classified into the covalent-bond, the radical-pair, and the dissociation region, as illustrated in Figure 3A. The covalent-bond region is typified by strong orbital interactions ($T_i \cong 1$), a large HOMO−LUMO gap in **2** (**3**), and a closed-shell pair $\psi_i^+ \cong \psi_i^- = \phi_i$ ($\theta \cong 0$). On the other hand, the SOMOs of **1** hardly interact with each other in the dissociation region ($T_i \cong 0$, $\theta \cong \pi/4$); $\psi^+ \cong \chi_a$ and $\psi^- \cong \chi_b$, where χ_c (c = a or b) is the SOMO of **1**. In the radical-pair region, two SOMOs in **2** (**3**) show weak orbital interactions ($0 < T_i < 1$), resulting in an antiferromagnetic coupling. The SOMO−SOMO overlap effect should be considered to account for the magnetic interactions in **3** because the experimental distance (R = 3.3 Å) of **2** is in the radical-pair region.[18] The broken symmetry MO picture, $\psi_i^+ \neq \psi_i^-$, is useful for pictorial understanding of the intermediate covalent bonds in **2** or **3**. Figure 3B gives a qualitative picture for α and β MOs in the three regions, which vary from symmetry-adapted MOs through broken symmetry MOs to SOMOs of fragment radicals such as **1**.

Computational Procedures

In this study, UB2LYP calculations were performed for **2** and **3** with the 6-31G basis set.[21] NOs and the occupation numbers were determined by eq 6. We also evaluated the J_{ab} values for **3** by the CASSCF method, and these results were utilized for the estimate of the relative contribution between SOMO−SOMO overlap and spin polarization effects. Other hybrid DFT (UB3LYP) and pure DFT (UBLYP) calculations were also carried out for **2** and **3** with the above basis sets (Tables S1 and S3). Previously, we have already examined the dependence of J_{ab} values on the calculation methods and the basis sets, indicating that the present basis sets are useful enough for qualitative examination of them.[10,22]

In the DFT calculations, exchange-correlation potentials are generally defined by

$$E_{XC} = C_1 E_X^{HF} + C_2 E_X^{Slater} + C_3 \Delta E_X^{Becke88} + C_4 E_C^{VWN} + C_5 \Delta E_C^{LYP} \tag{8}$$

where E_X^{HF} is the Hartree−Fock exchange, E_X^{Slater} is the Slater exchange, $\Delta E_X^{Becke88}$ is the gradient part of exchange functional of Becke,[12a] E_C^{VWN} is the correlation functional of Vosko, Wilk, and Nusair,[23] and ΔE_C^{LYP} is the correlation functional of Lee, Yang, and Parr,[12b] which includes the gradient of the density. The mixing coefficients (C_1, C_2, C_3, C_4, and C_5) are taken as (0.5, 0.5, 0.5, 1.0, and 1.0) for B2LYP,[22] respectively. All of the computations were carried out with Gaussian 94[24] and GAMESS[25] program packages.

The Origin of the Magnetic Interactions of 2

Calculated J_{ab} Values. To measure the magnitude of the magnetic interactions, we estimated the J_{ab} values for **2** and **3a**. The geometries of **2** were taken from the X-ray crystallographic results[3] as shown in Figure 1. We utilized standard parameters for **3a** to investigate the model dependence. The

(19) (a) Yamaguchi, K.; Okumura, M.; Takada, K.; Yamanaka, S. *Int. J. Quantum Chem. Symp.* **1993**, *27*, 501. (b) Yamaguchi, K.; Okumura, M.; Mori, W.; Maki, J.; Takada, K.; Noro, T. *Chem. Phys. Lett.* **1993**, *210*, 201.
(20) Takano, Y.; Kitagawa, Y.; Onishi, T.; Yoshioka, Y.; Yamaguchi, K.; Koga, N.; Iwamura, H. *J. Am. Chem. Soc.* **2002**, *124*, 450.
(21) Hehre, W. J.; Ditchfild, R.; Pople, J. A. *J. Chem. Phys.* **1972**, *56*, 2257.
(22) Takano, Y.; Taniguchi, T.; Isobe, H.; Kubo, T.; Morita, Y.; Yamamto, K.; Nakasuji, K.; Takui, T.; Yamaguchi, K. *Chem. Phys. Lett.* **2002**, *358*, 17.
(23) Vosko, S. H.; Wilk, L.; Nusair, M. *Can. J. Phys.* **1980**, *58*, 1200.
(24) Frisch, M. J.; Trucks, G. W.; Schlegel, H. B.; Gill, P. M. W.; Johnson, B. G.; Robb, M. A.; Cheeseman, J. R.; Keith, T. A.; Petersson, G. A.; Montgomery, J. A.; Raghavachari, K.; Al-Laham, M. A.; Zakrzewski, V. G.; Ortiz, J. V.; Foresman, J. B.; Cioslowski, J.; Stefanov, B. B.; Nanayakkara, A.; Challacombe, M.; Peng, C. Y.; Ayala, P. Y.; Chen, W.; Wong, M. W.; Andres, J. L.; Replogle, E. S.; Gomperts, R.; Martin, R. L.; Fox, D. J.; Binkley, J. S.; Defrees, D. J.; Baker, J.; Stewart, J. P.; Head-Gordon, M.; Gonzalez, C.; Pople, J. A. *Gaussian 94*, revision E.3; Gaussian Inc.: Pittsburgh, PA, 1995.
(25) Schmidt, M. W.; Baldridge, K. K.; Boatz, J. A.; Elbert, S. T.; Gordon, M. S.; Jensen, J. J.; Koseki, S.; Matsunaga, N.; Nguyen, K. A.; Su, S.; Windus, T. L.; Dupuis, M.; Montgomery J. A. *J. Comput. Chem.* **1993**, *14*, 1347.

Table 1. Effective Exchange Integrals (J_{ab})[a] for **2** and **3a**

model	UB2LYP	CASSCF {*m*, *m*}
2	−1505	
3a	−1470	−2266[b] (−3417)[c]

[a] J_{ab} values are in cm^{-1}. [b] $m = 2$. [c] $m = 6$.

C−C and C−H bond distances were assumed to be 1.40 and 1.08 Å, respectively. All of the bond angles were supposed to be 120°.[26]

Table 1 summarizes the J_{ab} values for **2** and **3a** using eq 2.[27] All of the J_{ab} values show strong intermolecular antiferromagnetic interactions consistent qualitatively with the SQUID measurements.[3−5] The difference in J_{ab} values between models **2** and **3a** is small, indicating that the substitution of *tert*-butyl groups with H atoms is not so significant for J_{ab}. Because CASSCF {2, 2} estimates the contribution of the SOMO−SOMO overlap effect (J_{ab}(OO)) to the magnetic coupling, the SOMO−SOMO overlap effect plays an important role in the antiferromagnetic interactions for **2** and **3a**. However, the absolute value by CASSCF {2, 2} is larger than those by UB2LYP, which includes the spin polarization and electron correlation effects. CASSCF {6, 6} provides larger $|J_{ab}|$ values than CASSCF {2, 2}, and these results are far different from the experimental values.[3−5] This is because the inclusion of π-electrons and π-orbitals is insufficient to evaluate the spin polarization and electron correlation effects. The more extended CASSCF followed by CASPT2 is inevitable for quantitative discussion of the J_{ab} values.[9d]

Figure 4A illustrates the J_{ab} values for **3a** with the change in the intermolecular distance *R* by UB2LYP.[28] The J_{ab} values are negative in the whole region, showing the intermolecular antiferromagnetic interactions. The $|J_{ab}|$ rapidly increases with decreasing *R*. This trend is independent of the employed computational methods (Table S2). Figure 4B depicts the potential curves in the HS, LS, and AP-LS states for **3a** with varying *R*. The potential energy surfaces in HS and LS are repulsive, while the potential minimum with the AP correction is located at $R = 3.5$ Å, in qualitative agreement with the experiment ($R = 3.3$ Å).[3−5] This clearly demonstrates an important role in elimination of the HS component from the broken symmetry LS solution by our AP procedure as shown in eq 3.

Spin Density Distributions. In broken symmetry approaches, spin density distributions appear even for the LS singlet state. As shown previously,[10a] the spin densities are not strictly related to real spin populations, but they are useful indices to describe the magnitude of electron and spin correlations in strongly correlated finite systems, approximately providing the SDP terms in the extended McConnell model. Table 2 lists the spin density distributions for **2** and **3a**. Sites a−d and a′−d′ in **2** and **3a** are denoted in **3a** of Figure 1. These results indicate that the sign of spin densities alternatively changes, showing

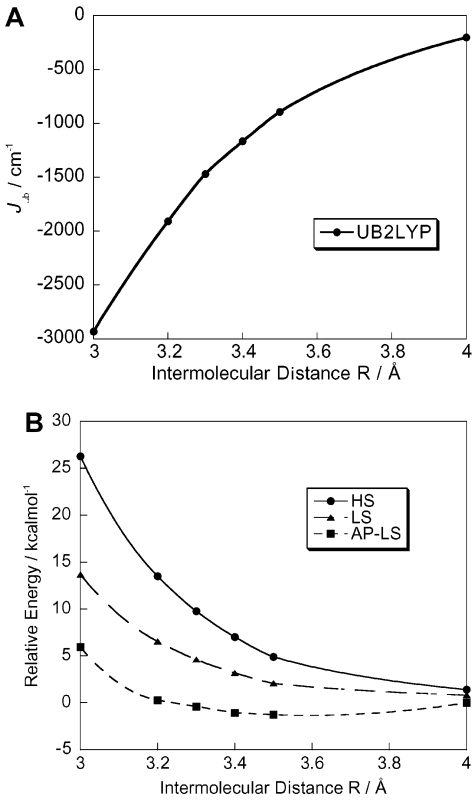

Figure 4. The J_{ab} values for **3a** by UB2LYP (**A**) and the potential curves for **3a** by UB2LYP (**B**), varying the intermolecular distance *R*.

Table 2. Spin Density Distributions[a] for Phenalenyl Radical Dimeric Pair **2** and **3a** in the LS State at $R = 3.3$ Å

model	a	b	c	d	a′	b′	c′	d′
2	+0.374	−0.251	−0.249	+0.177	−0.373	+0.250	+0.248	−0.177
3a	+0.448	−0.328	−0.328	+0.267	−0.448	+0.328	+0.328	−0.267

[a] Sites a (a′)−d (d′) are shown in Figure 1.

that the SDP term as well as the OO term contributes to the antiferromagnetic coupling for **2** and **3a**. The average of the absolute values of the spin population on the carbon atoms in **3a** is about 0.38, showing a diradical character and a weak spin polarization effect. The spin density distributions of **2** are similar to those of **3a**, implying that *tert*-butyl groups do not affect the spin densities as well as J_{ab} values. In other words, the SDP term (spin polarization effect) of the magnetic interactions for **2** is nearly equal to that for **3a**.

Molecular and Natural Orbital Analysis. MOs and the occupation numbers provide us insight into understanding the origin of the strong antiferromagnetic interactions for **2** and **3a**. Figure 5A and B shows shapes of the α and β SOMOs for **2** and **3a** in the LS state by UB2LYP, respectively.[29] The SOMOs are partially delocalized over the dimeric pair. Because delocalized α and β SOMOs provide orbital overlaps, the magnetic interactions for **2** and **3a** are antiferromagnetic.

Table 3 summarizes the occupation numbers of HOMO, SOMOs, and LUMO for **2** and **3a** in the LS state by UB2LYP and CASSCF calculations. From the occupation numbers of SOMO − 1 and SOMO + 1, the T_{SOMO} values for **2** and **3a**,

(26) (a) Takano, Y.; Soda, T.; Kitagawa, Y.; Yoshioka, Y.; Yamaguchi, K. *Chem. Phys. Lett.* **1999**, *301*, 309. (b) Takano, Y.; Soda, T.; Kitagawa, Y.; Onishi, T.; Yoshioka, Y.; Yamaguchi, K. *Int. J. Quantum Chem.* **2000**, *80*, 681.

(27) The total energy and angular momentums and the J_{ab} values by UHF, UB2LYP, MEDF (UB2′LYP), UB3LYP, UBLYP, UNO CASCI {2, 2} and {6, 6}, and CASSCF {2, 2} and {6, 6} calculations are summarized in Table S1.

(28) The total energies and total spin angular momentum for the HS, LS, and AP-LS states, and the J_{ab} values by UB2LYP and UB3LYP for **3a** with the change of the intermolecular distance *R* by calculations are listed in Table S2.

(29) The α and β SOMOs of **2a** and **3** by UHF (**A**), UB2LYP (**B**), UB2′LYP (**C**), UB3LYP (**D**), and UBLYP (**E**) are displayed in Figures S1 and S2, respectively.

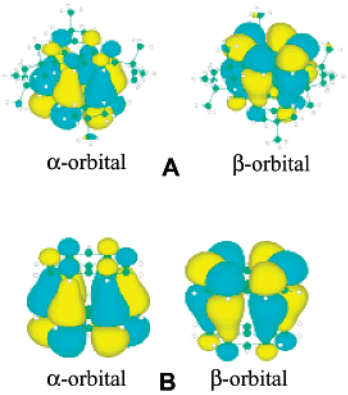

Figure 5. The α and β SOMOs of **2** (A) and **3a** (B) by UB2LYP in the LS state, respectively.

Table 3. Occupation Numbers of HOMO, SOMOs, and LUMO for **2** and **3a** in the LS State at $R = 3.3$ Å

model	method	HOMO	SOMO + 1	SOMO − 1	LUMO
2	UB2LYP	1.971	1.445	0.555	0.029
3a	UB2LYP	1.968	1.403	0.597	0.032
	CASSCF {2, 2}	2.000	1.719	0.281	0.000
	CASSCF {6, 6}	1.974	1.697	0.306	0.025

which show the strength of the orbital interactions between the magnetic SOMOs (α and β SOMOs), are 0.445 and 0.403, respectively. Because the absolute values of J_{ab} increase with an increase in T_{SOMO}, the SOMO−SOMO overlap effect is essential for the magnetic interaction for **2** and **3a**. A small difference in T_{SOMO} values between **2** and **3a** leads to the similar estimate of the OO term of the J_{ab} values. The T_{SOMO} values by CASSCF are larger than those by UB2LYP, consistent with the tendency that the absolute J_{ab} value by the former is larger than that of the latter. UB2LYP can deal with the SOMO−SOMO overlap effect appropriately because of 50% mixing of the BLYP component. Using the occupation numbers of HOMO and LUMO, we found that the T_{HOMO}'s for the HOMOs (ψ^{+}_{HOMO} and ψ^{-}_{HOMO}) by UB2LYP and CASSCF {6, 6} calculations are 0.968 and 0.974, respectively. UB2LYP shows that such reductions of the occupation numbers ($T_i < 1.0$) are not negligible for many other orbitals except for HOMO, suggesting the necessity of the extended CASSCF calculations followed by CASPT2 for quantitative purpose.

Origin of the Magnetic Interaction of 2. We discuss the origin of the antiferromagnetic interaction for **2** on the basis of the extended McConnell model. UB2LYP provides J_{ab} values close to the experimental ones, showing that DFT employing appropriate exchange-correlation functionals is practically useful for elucidation of electronic and magnetic properties. Considering the occupation number of HOMO and LUMO, the SOMO−SOMO overlap effects are more effective to the magnetic interactions for **2** and **3a** than are the spin polarization effects. The differences between **2** and **3a** are small in J_{ab} values, spin density, MOs, and NOs, indicating that the substitution of *tert*-butyl groups with H atoms is not so sufficient for the magnetic interaction and the electronic structure of **2**.

Stacking Effects for the Magnetic Interaction of Phenalenyl Radical Dimeric Pair

J_{ab} Values. To determine which stacking type contributes to the intermolecular ferromagnetic interaction, the stacking effects

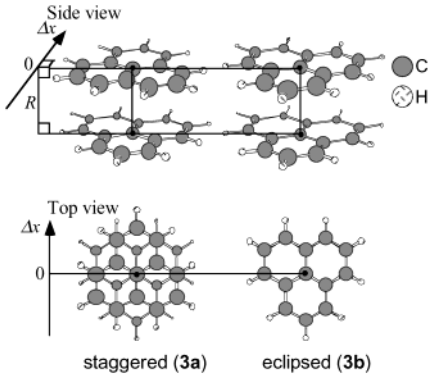

Figure 6. Side and top views of staggered (**3a**)- and eclipsed (**3b**)-stacking modes for the phenalenyl radical dimeric pair.

were investigated in terms of the J_{ab} values, the SOMO−SOMO overlap effect, and the spin polarization effect. We considered the intermolecular magnetic interactions for **3** because the phenalenyl part was more important for the magnetic coupling as shown above. The distance R between the two phenalenyl radicals was assumed to be 3.3 Å because these parameters were close to the experimental values. Considering the SOMO−SOMO overlap effects, we found that the upper phenalenyl group of the staggered-stacking (the same stacking mode as experiment) (**3a**) and eclipsed-stacking (**3b**) phenalenyl radical dimeric pair was offset in parallel to the lower phenalenyl group as shown in Figure 6. UB2LYP/6-31G calculations were performed with a shifting of the distance, Δx.

Figure 7A and B shows the variation of the J_{ab} values for **3a** and **3b**, varying Δx, respectively.[30] In Figure 7A and Table 4, the J_{ab} values are 86.85 and 346.1 cm^{-1} by UB2LYP calculation at $\Delta x = -2.8$ (**3c**) and 1.4 Å (**3d**), respectively, indicating ferromagnetic interactions between the phenalenyl radicals. Similarly, the J_{ab} values by UB2LYP are 133.0 cm^{-1} at $\Delta x = -1.4$ and 1.4 Å (**3e**), also showing ferromagnetic couplings as displayed in Figure 7B.

CASSCF {2, 2} calculations estimate the contribution of the SOMO−SOMO overlap effects to the magnetic couplings. The J_{ab} values by CASSCF {2, 2} for **3a** and **3b** are approximately -2000 cm^{-1}, showing strong antiferromagnetic interactions. The SOMO−SOMO overlap effects are responsible for strong antiferromagnetism for **3a** and **3b**. On the other hand, $|J_{ab}|$ values for **3c**−**3e** reduce remarkably, implying that the SOMO−SOMO overlap effects become weak for the magnetic interaction. Especially, the overlap effect for **3d** shows an intermolecular ferromagnetic interaction because of Hund's rule.

Molecular and Natural Orbital Analysis. MO pictures seem to be suitable for a deep understanding of the magnetic interaction for models **3a**−**3e**.[10,15] Figure 8 shows the shapes of the α and β SOMOs for **3a**−**3e** in the LS state, respectively. The SOMOs for **3a**, **3b**, and **3d** are partially delocalized over the dimeric pair, showing that delocalized α and β SOMOs of **3a** and **3b** provide large orbital overlaps, while those of **3d** hardly yield orbital overlap (see Table 5) because each SOMO is out of phase from each other. The SOMOs for **3c** and **3e** are

(30) The total energies and total spin angular momentum for the HS and LS states and the J_{ab} values calculated for **3z** (**z** = **a**−**e**) by UB2LYP, UB3LYP, UNO CASCI {2, 2}, and CASSCF {2, 2} calculations are summarized in Table S3.

(31) (a) Kitagawa, Y.; Kawakami, T.; Yamaguchi K. *Mol. Phys.* **2002**, *100*, 1829. (b) Kitagawa, Y.; Soda, T.; Shigeta, Y.; Yamanaka, S.; Yoshioka, Y.; Yamaguchi, K. *Int. J. Quantum Chem.* **2001**, *84*, 592.

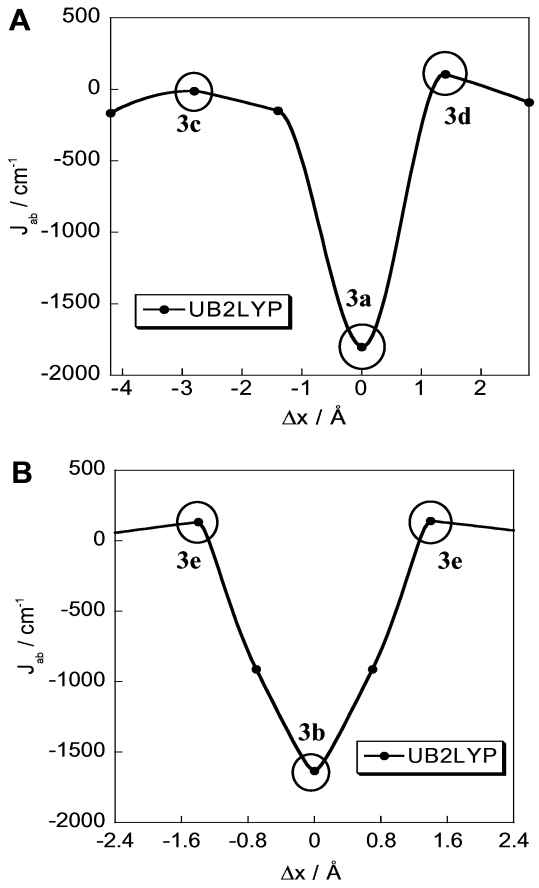

Figure 7. The J_{ab} values for **3a** (A) and **3b** (B) with the variation of the shifting distance Δx by UB2LYP.

Table 4. Effective Exchange Integrals (J_{ab})[a] for **3a**−**3e**

stacking	UB2LYP	CASSCF {2, 2}
3a	−1470	−2266
3b	−1633	−2132
3c	86.85	−15.70
3d	346.1	71.58
3e	133.0	−4.272

[a] J_{ab} values are in cm^{-1}.

almost localized over one phenalenyl radical, indicating that the SOMO−SOMO overlap effects between the phenalenyl dimer decrease remarkably. The SOMO−SOMO overlap effects dominate the magnetic interactions between phenalenyl radicals for **3a** and **3b**, while they become small for the magnetic couplings for **3c**−**3e**.

Table 5 summarizes the occupation numbers of HOMO, SOMO, and LUMO for phenalenyl radical dimeric pairs **3a**−**3e** in the LS state. T_{SOMO} values increase in order: **3c** ≅ **3d** ≅ **3e** ≪ **3a** ≅ **3b**. The J_{ab} values show strong antiferromagnetic couplings as T_{SOMO} values become larger. The occupation numbers of HOMO and LUMO indicate that the spin polarization effects are weak for all of the stacking types. To obtain organic ferromagnetic crystals, we first need to stack phenalenyl radicals with small T_{SOMO} values, small SOMO−SOMO overlaps. When the SOMO−SOMO overlap is relatively weak, the intermolecular Coulombic exchange (Hund's rule) term and spin polarization effect play important roles in the magnetic interactions.

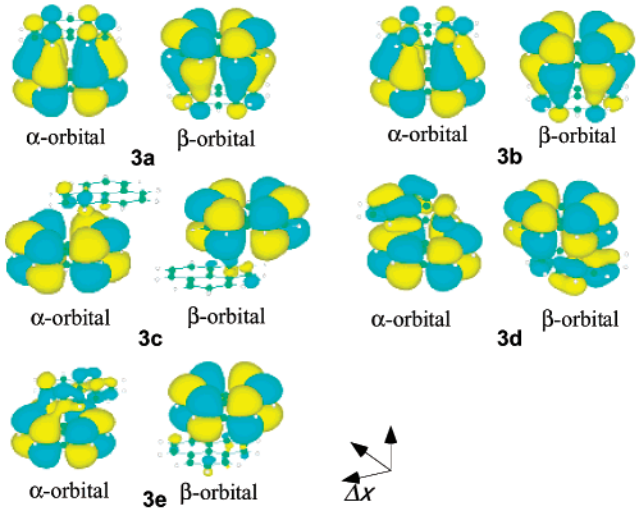

Figure 8. The α and β SOMOs of **3a**−**3e** by UB2LYP in the LS state are shown.

Table 5. Occupation Numbers of HOMO, SOMOs, and LUMO for **3a**−**3e** in the LS State

method	stacking	HOMO	SOMO − 1	SOMO + 1	LUMO
UB2LYP	**3a**	1.968	1.403	0.597	0.032
	3b	1.960	1.389	0.611	0.040
	3c	1.968	1.065	0.935	0.032
	3d	1.967	1.083	0.917	0.033
	3e	1.966	1.082	0.918	0.034

Table 6. Spin Density Distributions[a] for **3a**−**3e** in the More Stable State at R = 3.3 Å

model	a	b	c	d	a′	b′	c′	d′
3a (LS)	+0.448	−0.328	−0.328	+0.267	−0.448	+0.328	+0.328	-0.267
3b (LS)	+0.462	−0.344	−0.344	+0.287	−0.462	+0.344	+0.344	-0.287
3c (HS)	+0.438	−0.305	−0.273	+0.209	+0.438	−0.305	−0.273	+0.209
3d (HS)	+0.426	−0.294	−0.267	+0.203	+0.426	−0.294	−0.267	+0.203
3e (HS)	+0.488	−0.352	−0.351	+0.286	+0.486	−0.356	−0.356	+0.289

[a] Sites a (a′)−d (d′) are shown in Figure 1.

Spin Density Distributions. Spin density distribution enables us to estimate the intermolecular Coulombic exchange and spin polarization effects (SDP term), qualitatively.[9] The spin densities on carbon atoms in the LS state for **3a** and **3b** and in the HS state for **3c**−**3e** are listed in Table 6. Figure 9 shows the schematic presentation of the spin density distributions for **3a**−**3e**. Intermolecular magnetic interactions of larger spin densities (dots line) for **3a** and **3b** induce strong antiferromagnetic contributions of the spin polarization effects of the phenalenyl radical dimeric pair. Although the numbers of the nearest intermolecular magnetic coupling are 13 and 7 for **3a** and **3b**, respectively, the J_{ab} values are close to each other. It indicates that the SOMO−SOMO overlap effects are more dominant for the intermolecular magnetic coupling for **3a** and **3b** than spin polarization effects. On the other hand, **3c**−**3e** in Figure 9 show that intermolecular magnetic interactions between larger and smaller spin densities and between smaller and smaller ones (dots line) lead to the alignment of larger spins in the same direction, indicating ferromagnetic couplings. The numbers of the nearest intermolecular spin interactions, in other words, the number of dotted lines, are 6, 10, and 5 for **3c**, **3d**, and **3e**, respectively, showing the similar tendency as the J_{ab} values: J_{ab} (**3c**) ≅ J_{ab} (**3e**) < J_{ab} (**3d**). These results imply that

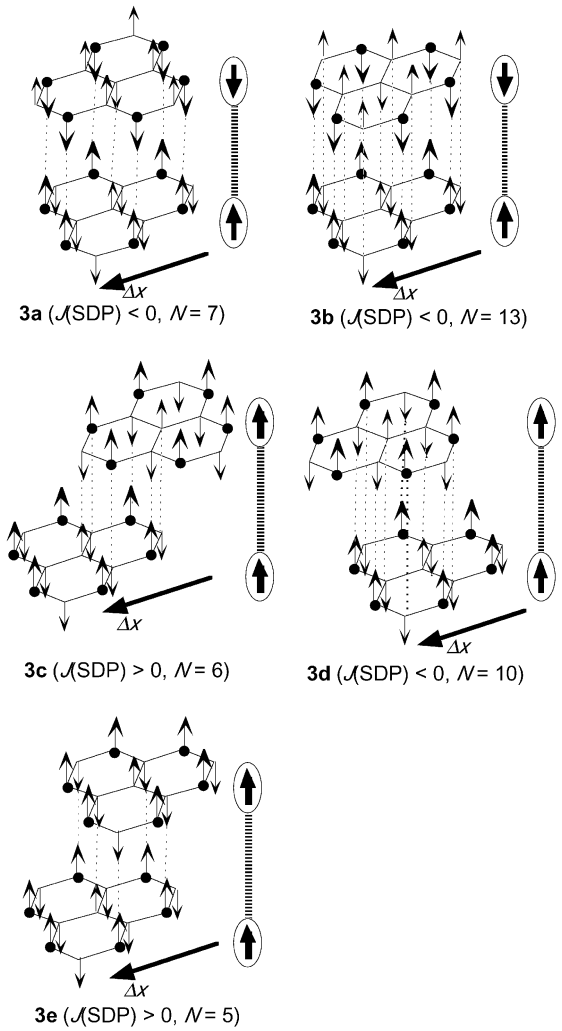

Figure 9. Schematic pictures of spin densities of **3a**−**3e** estimated by DFT calculations and magnetic interactions of **3a**−**3e** predicted by spin polarization effects. Large arrows depict the large spin densities at α-positions of phenalenyl radicals, while small arrows show the small spin densities induced by large spin densities. Dotted lines represent intermolecular spin interactions.

ferromagnetic interactions for **3c**, **3d**, and **3e** are responsible for the spin polarization effects.

Stacking Effect of the Magnetic Interaction for 3. The J_{ab} values for **3c**−**3e** show ferromagnetic interactions, because of the small orbital overlap and the ferromagnetic spin polarization effects. In this study, stacking mode **3d** is the best for the phenalenyl radical dimeric pair to obtain ferromagnetic organic crystals because of the ferromagnetic OO (Hund's effect) and spin polarization effects. The CASSCF {2, 2} results suggest that Hund's effect is predominant for the SOMO−SOMO overlap interaction in this stacking. The above results suggest that the J_{ab} values show strong antiferromagnetic interactions for **3a** and **3b** because of the large SOMO−SOMO overlap effects and ferromagnetic couplings for **3c**−**3e** due to the small SOMO−SOMO overlap effects and the ferromagnetic spin polarization effects. These results indicate that stacking modes with small orbital overlap and ferromagnetic intermolecular spin alignment are crucial for establishing intermolecular ferromagnetic preference in the crystal. Chemical modification of new phenalenyl radicals with the potential staggered- and eclipsed-stacking modes is underway.

Discussion

Extended McConnell Model. In addition to the McConnell SDP term, we have considered an important role in the SOMO−SOMO overlap effect for the molecular design of ferromagnetic organic crystals, proposing the extended McConnell model.[9] In this paper, on the basis of the extended McConnell model, we investigated the stacking effects for the magnetic interaction of the phenalenyl radical dimeric pair by UB2LYP calculation with the variation of the SOMO−SOMO overlap. The calculated results indicate that the stacking modes of this dimeric pair with a small SOMO−SOMO overlap and ferromagnetic spin polarization effects show ferromagnetic interactions. The CASSCF results supported our extended McConnell model.[9]

Hybrid DFT. The computational results indicate that we can choose the best hybrid UDFT procedure involving the SOMO−SOMO overlap and other effects in a well-balanced manner, leading to the magnetically effective density functional (MEDF) approach.[31] In this paper, UB2LYP has been utilized for qualitative study of J_{ab} values for radical dimer as in the cases of other strongly correlated electron systems.[32] Generally, MEDF is made so as to reproduce the occupation numbers by post HF such as coupled-cluster (CC) SD(T) and CASPT2 for small model. In this study, we need to perform the CASSCF {26, 26} calculation for **3a**. However, it is difficult for our computer systems. Thus, we may utilize the occupation numbers by CASSCF {6, 6} calculations for **3a** to determine MEDF (UB2′LYP). Although the UB2′LYP calculations clearly demonstrate the necessity of active controls of stacking modes for ferromagnetic spin alignments (Table S1), UB2′LYP is never regarded as an alternative to CASSCF {26, 26}. Therefore, many other efforts such as multireference (MR) DFT[33] are necessary for further improvement of DFT.

Concluding Remarks

We performed UB2LYP calculations for the phenalenyl radical dimeric pairs **2** and **3a** to elucidate the origin of the magnetic interactions and the nature of the chemical bonds and to obtain the ferromagnetic stacking modes. MO analysis of UB2LYP solutions was very useful for this purpose. Our conclusions are as follows: (i) Dimeric pair **2** showed a strong intermolecular antiferromagnetic coupling because of the large SOMO−SOMO overlap interaction. (ii) Because *tert*-butyl groups introduced at three *β*-positions hardly contribute to the magnetic coupling, *tert*-butyl groups mainly played steric hindrances in a crystalline state. (iii) The spin projection for the broken-symmetry LS solution was essential for depicting the reasonable potential curve for **2** (**3a**). (iv) The chemical bonds between the phenalenyl radicals showed the intermediate character between bond dissociation and covalent bonding. (v) The stacking modes with the small SOMO−SOMO overlap effect (J_{ab}(OO) in eq 5) and the ferromagnetic Coulombic exchange and spin polarization effects (J_{ab}(SDP)) provided ferromagnetic interactions. (vi) Hybrid DFT and CASSCF results verified the extended McConnell model[9] as one of the guiding principles for organic ferromagnets.

Acknowledgment. We would like to thank Ms. Fusayo Saeki for helpful discussion. This work has been supported by a Grant-

(32) Onishi, T.; Takano, Y.; Kitagawa, Y.; Kawakami, T.; Yoshioka, Y.; Yamaguchi, K. *Polyhedron* **2001**, *20*, 1177.
(33) Isobe, H.; Takano, Y.; Kitagawa, Y.; Kawakami, T.; Yamanaka, S.; Yamaguchi, K.; Houk, K. N. *Mol. Phys*. **2002**, *100*, 717.

in-Aid for Scientific Research on Priority Areas (No. 10149105 "Metal Assembled Complexes") from the Ministry of Education, Culture, Sports, Science, and Technology, Japan. Y.T. was also supported by Research Fellowships of Japan Society for the Promotion of Science for Young Scientists.

Supporting Information Available: Total energies and total angular momentums and the J_{ab} values for **2** and **3a** by UHF, UB2LYP, UB2′LYP, UB3LYP, UBLYP, UNO CASCI, and CASSCF calculations (Table S1); total energies and total spin angular momentum for the HS, LS, and AP-LS states, and effective exchange integrals calculated for **3a** with the change of the intermolecular distance R by UB2LYP and UB3LYP calculations (Table S2); total energies and total spin angular momentum for the HS and LS states, and the J_{ab} values calculated for **3z** (**z** = **a**−**e**) by UB2LYP, UB3LYP, UNO CASCI {2, 2}, and CASSCF {2, 2} calculations (Table S3); the α and β SOMOs of **2a** (Figure S1) and **3** (Figure S2) by UHF (A), UB2LYP (B), UB2′LYP (C), UB3LYP (D), and UBLYP (E) (PDF). This material is available free of charge via the Internet at http://pubs.acs.org.

JA0177197